Recent Experimental Progress in the Area of Electron Cyclotron Resonant Heating (ECRH) and Electron Cyclotron Current Drive (ECCD) in Magnetically Confined Fusion Plasmas

Hartmut Zohm

Max-Planck-Institut für Plasmaphysik, D-85748 Garching, Germany, EURATOM Association

Abstract: A review of recent experimental results in the area of ECRH and ECCD is given. Special emphasis is put on the recent developments of new schemes in which EC waves can heat and drive current in magnetically confined fusion plasmas. These comprise scenarios to overcome the density cutoff experienced in application of the classical O1 and X2 scheme as well as to increase the current drive efficiency of EC waves while maintaining their good localization. In particular, we discuss recent experimental progress in tokamaks, stellarators and spherical tori in the areas of the O2, X3 and EBW schemes (mostly OXB scheme) as well as experiments in which the combination of ECCD with Lower Hybrid Current Drive (LHCD) leads to a synergetic increase of the ECCD efficiency. A particular application of ECCD that has recently received a lot of attention and is therefore reviewed in this paper is the suppression of Neoclassical Tearing Modes (NTMs) by ECCD. We show that the theoretically predicted requirements for ECCD in terms of deposition (maximising the ECCD driven current density) and injection in phase with the O-point of the magnetic island associated with the NTM (which is needed when the island width falls below the deposition width) have been verified experimentally. Also, many of the elements needed for constructing a reliable, feedback controlled NTM suppression system for ITER based on ECCD have now been demonstrated experimentally and the next step, which is their integration into a reliable scheme, is well within reach.

1. Introduction

Heating and Current Drive by Electron Cyclotron (EC) waves in magnetically confined plasmas is by now a well-established method, with the basic mechanisms of microwave propagation, absorption and current drive employing the classical schemes, i.e. first harmonic ordinary (O1) mode or second harmonic extraordinary (X2) mode, well described by theory [1], [2]. The field has benefited significantly from recent progress in development of high power microwave sources, most prominently the gyrotron, and the corresponding technology to transmit and launch microwave beams into the plasma [3], [4].

Therefore, the main interest in research in the field of ECRH and ECCD in high temperature fusion plasmas is either devoted to establishing new heating and current drive schemes, other than the conventional O1 or X2, or to the use of ECRH and ECCD for sophisticated applications to control plasma parameters. In particular the localized heating and current drive that is possible by ECRH and ECCD has led to applications in confinement as well as in tailoring MHD stability. An earlier review of this area can be found in [5]; since then, major progress in this field has especially been in the area of the suppression of Neoclassical Tearing Modes (NTMs). The emphasis of this review is therefore on new schemes for ECRH and ECCD and on the application of classical ECCD schemes to NTM suppression. For a review of the other fields, we refer to [1], [2], and [5].

2. Development of new schemes for ECRH and ECCD

As pointed out above, the 'classical' O1 and X2 schemes are well documented and understood, so that they are not part of this review. There are two main drawbacks, for these schemes,

namely the upper density limit due to wave cutoff and the relatively poor current drive efficiency. Recent work has addressed both limitations, trying to establish schemes that improve both accessibility and current drive efficiency.

Concerning accessibility, cutoff occurs when the microwave of frequency ν_{wave} reaches, for O-mode, the plasma frequency ν_{pe} or, for X-mode the fast X-mode cutoff frequency ν_{fc} defined by

$$\nu_{pe} = \frac{1}{2\pi}\sqrt{\frac{n_e e^2}{m_e \varepsilon_0}} \qquad \text{and} \qquad \nu_{fc} = \sqrt{\frac{\nu_{ce}^{\,2}}{4} + \nu_{pe}^{\,2}} + \frac{\nu_{ce}}{2} \tag{1}$$

where n_e is the electron density and m_e the relativistic electron mass. The electron cyclotron frequency is defined as

$$\nu_{ce} = eB/(2\pi m_e) \tag{2}.$$

By equating the electron cyclotron frequency to the respective cutoff frequency, one obtains, for the ℓ-th harmonic, the cutoff density

$$n_{e,co} = l^2 \frac{\varepsilon_0 B^2}{m_e} \qquad \text{or, in SI-units } n_{e,co} = 9.65 \times 10^{18}\ \text{m}^{-3}\ \ell^2 B^2\ [\text{T}] \qquad \text{in O-mode} \tag{3}$$

$$n_{e,co} = l(l-1)\frac{\varepsilon_0 B^2}{m_e} \quad \text{or, in SI-units } n_{e,co} = 9.65 \times 10^{18}\ \text{m}^{-3}\ \ell(\ell\text{-}1) B^2\ [\text{T}] \text{ in X-mode} \tag{4}.$$

Since in a typical tokamak plasma, densities around 10^{20} m^{-3} are sought and on the other hand, usually only $\ell=1$ is optically thick enough for single pass absorption in the O-mode, it follows that this scheme is only relevant above ~ 3 T. The situation is a bit more relaxed for the X-mode since here, also the 2nd harmonic is usually optically thick, yielding a factor of 2 higher value for X2 than for O1. This allows access to densities around 10^{20} m^{-3} for fields down to 2 T, but at a lower field, again the cutoff represents a severe restriction on the operational range.

A possible way out is the use of higher harmonics, but then one has to deal with the problem of incomplete single-pass absorption. As an example of this scheme, we discuss in the next subsection the work done on O2 and X3 mode. For a much lower field, as is the case in the spherical torus or the reversed field pinch, or for much higher density, as is typical for stellarators, the OXB conversion scheme is the best candidate. This is discussed in subsection 2.2. The OXB scheme also promises higher current drive efficiency than the usual schemes.

Concerning the current drive efficiency, one can look at the general resonance condition for electrons with parallel velocity $v_{e||}$ in a magnetic field interacting with an electromagnetic wave whose wave number parallel to the magnetic field is $k_{||}$ (or equivalently, whose parallel index of refraction is $N_{||} = k_{||}/k_0 = ck_{||}/(2\pi\nu_{wave})$ for electron cyclotron waves)

$$\nu_{wave} - l\nu_{ce} - \frac{k_{||}v_{||}}{2\pi} = \nu_{wave}\left(1 - N_{||}\frac{v_{||}}{c}\right) - l\nu_{ce} = 0 \tag{5}$$

which shows that for $\ell = 0$, the electrons in resonance have to have a velocity of the order of the speed of light whereas for $\ell \neq 0$, electrons can be much slower due to the cyclotron

resonance. The former case corresponds to LHCD, which, via Landau damping, directly generates fast parallel electrons, whereas EC schemes work on the perpendicular energy of electrons with parallel velocity still in the vicinity of the thermal velocity via the Fisch-Boozer mechanism [6]. As a result, LHCD has about one order of magnitude higher CD efficiency than ECCD. Recent work combining LHCD and ECCD has shown significant synergy, i.e. the current driven by the two systems simultaneously can be substantially higher than the sum of the two currents driven individually. This is discussed in subsection 2.3.

2.1 Experiments using the O2 and X3-mode

Extensive experimental work on X-3 heating has been performed on the TCV tokamak [7]. The optical thickness in the X3 mode is smaller than that of X2 by a factor of $kT/(mc^2)$, so that absorption is not necessarily complete along the first path through the plasma. At TCV, the X3 wave was therefore launched from a top launcher positioned at the EC resonance, so that overlap of the beam path with the resonance is maximized, increasing the optical thickness approximately linearly with overlap length, as indicated in the left panel of Fig. 1. Such a scheme needs careful alignment of the beam, which in the case of TCV was provided by a feedback algorithm that continuously swept the launching mirror across the resonance to find the maximum absorption, as indicated from the maximum in electron temperature deduced from a two color Soft-X-Ray diagnostic. This scheme proved to be very efficient, allowing substantial plasma heating at X3 above the X2 cutoff. An example is shown in the right panel of Fig. 1, where an Ohmic H-mode is heated by about 1.4 MW of X3 ECRH. Calculations of the absorbed power predict that initially, about 35 % are absorbed, but due to the strong rise of the electron temperature, the stationary phase shows more than 70 % of absorption.

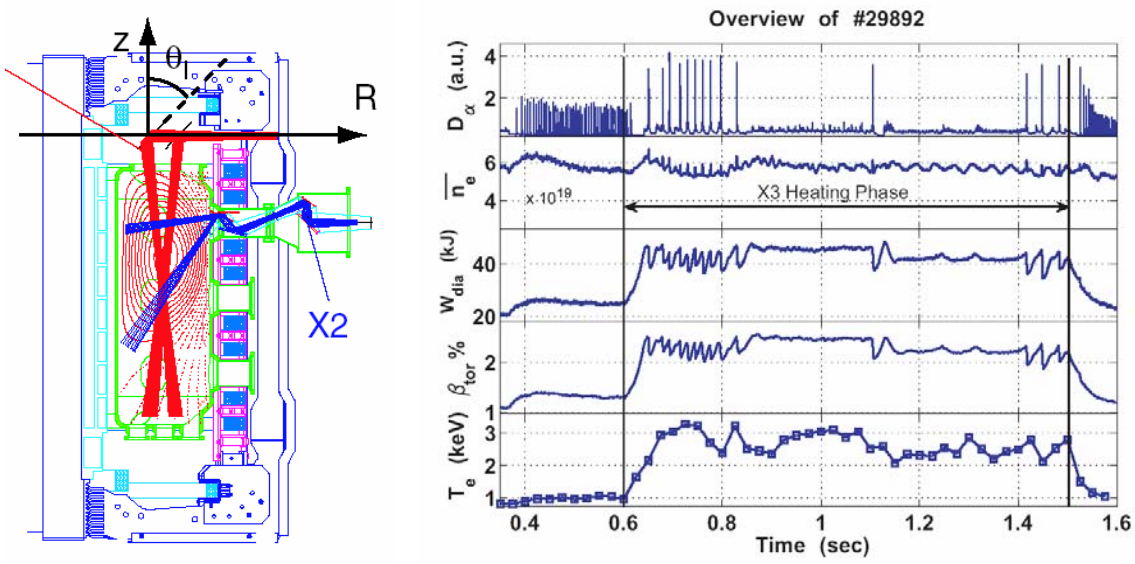

Fig. 1: X3-mode ECRH in the TCV tokamak: Launcher geometry (left) and H-mode discharge heated by X3 ECRH (right).

In general, the measured X3 absorption is often higher than the calculated one if a Maxwellian velocity distribution of the electrons is assumed. However, under the assumption of a suprathermal component, generated either by X2 preheat or by the X3 wave itself, the results can be brought to match. Moreover, hard X-ray measurements and high field side ECE on TCV give direct experimental evidence for the existence of such a suprathermal electron population [8]. Modulated injection allows to study the diffusion of the ECRH generated fast electrons both in velocity and in real space. Interestingly, the inferred spatial diffusion

coefficients seem to be well in excess of those valid for anomalous transport of thermal electrons.

Concerning the O2 scheme, there have been few experiments making use of this scheme. In TEXTOR, O2 heating was applied at densities above the X2 cutoff [9]. The inferred absorption of up to 60% under these conditions was in rough agreement with the calculated value. Experiments in the W7-AS stellarator [10] yielded an absorption higher than that calculated for single pass, which was attributed to multiple passes of the microwave after reflection on the inner wall. In addition, at higher density, absorption seemed to be even more enhanced (up to a factor of 2 above the calculated value). However, the experimental situation is not conclusive yet. For the W7-X stellarator, it is planned to install special reflecting structures on the inner wall that reflect the wave with the correct polarization for the second pass. Such structures have also been installed in ASDEX Upgrade to test the concept [11]. In none of these experiments was there a diagnostic of the electron distribution function and hence, nothing can be said about a possible role of suprathermals. However, the rough quantitative agreement with theoretical prediction may be taken as an indication that the O2 scheme could be attractive to larger machines which, due to higher density and temperature, will have larger single pass absorption anyway.

2.2 O-X-B conversion

The problem of high density cutoff of EC waves can be overcome by exciting Bernstein waves, because they have no density limitation. However, these electrostatic waves do not exist in vacuum and thus have to be generated in the plasma. This can be done with very high efficiency by using the slow X-B conversion at the upper hybrid resonance (UHR) layer with

$$\nu_{UH} = (\nu_{pe}^2 + \nu_{ce}^2)^{1/2} \tag{6}.$$

Thus, the problem comes down to generating a slow X-mode wave that travels to the UHR. Comparing (2) and (6), it can be seen that for a given frequency, the UHR layer is located further out in the minor radius than the cyclotron resonance as long as the density is finite. The slow X-mode exists below ν_{UH} down to its cutoff at

$$\nu_{sc} = \sqrt{\frac{\nu_{ce}^2}{4} + \frac{\nu_{pe}^2}{1 - N_{||}^2}} - \frac{\nu_{ce}}{2} \tag{7}$$

and can thus be used in the window $\nu_{sc} < \nu_{wave} < \nu_{UH}$, but at the boundary (where $\nu_{pe} \to 0$), ν_{UH} approaches ν_{ce} and thus the wave must be injected from the high field side if its frequency should be resonant with the first harmonic of ν_{ce} in the plasma core and still be below ν_{UH}. This has been successfully demonstrated in COMPASS-D [12]. However, high field side launch is usually technically not easy in toroidal fusion experiments and in addition, ν_{sc} must be smaller than the wave frequency along the whole path up to the UHR layer, so that the use of this scheme is restricted to below the cutoff density. Alternatively, one can make use of the O-X conversion that happens when the O-mode is injected obliquely at an angle so that its cutoff matches that of the slow X-wave at the conversion point. Equating ν_{sc} to ν_{pe} gives the condition $N_{||opt}^2 = \nu_{ce}/(\nu_{ce} + \nu_{wave})$ for optimum conversion where ν_{ce} has to be evaluated at the conversion point. The transmission efficiency for O-X conversion is given by

$$T_{OX} = \exp\left\{ -\pi k L \sqrt{\frac{\nu_{ce}}{2\nu}} \left[2(1+\frac{\nu_{ce}}{\nu})(N_{\|opt} - N_{\|})^2 + N_{\perp}{}^2 \right] \right\} \qquad (8)$$

where $L=n/\nabla n$ is the density gradient length. This implies that the density gradient length should not be much larger than the wavelength to obtain good conversion efficiency. The most severe restriction to obtaining a high value is that in reality, the plasma density will fluctuate so that the conversion layer is not smooth. A statistical analysis [13] shows that again, a higher fluctuation level can be tolerated for a steeper gradient while an increasing fluctuation amplitude decreases T_{OX}. Finally, it is worth mentioning that Bernstein waves should also be useful to drive current in a high temperature plasma, which makes them especially attractive to be used in configurations that need internal currents to sustain the configuration such as STs or RFPs. The predicted CD efficiency is higher than that of conventional ECCD [14] and this has been demonstrated in the inside launch experiment in COMPASS-D [12]. We note here that a third scheme, the direct X-B conversion exists for low field devices where the width of the evanescent region between the two layers can be comparable to the wave length and thus tunneling is possible in principle. However, in this scheme, the requirement for a steep density gradient and low fluctuations has been found to be more restrictive than for the OXB scheme so that we only treat the latter here. For more details see, e.g. the recent review by Laqua [15].

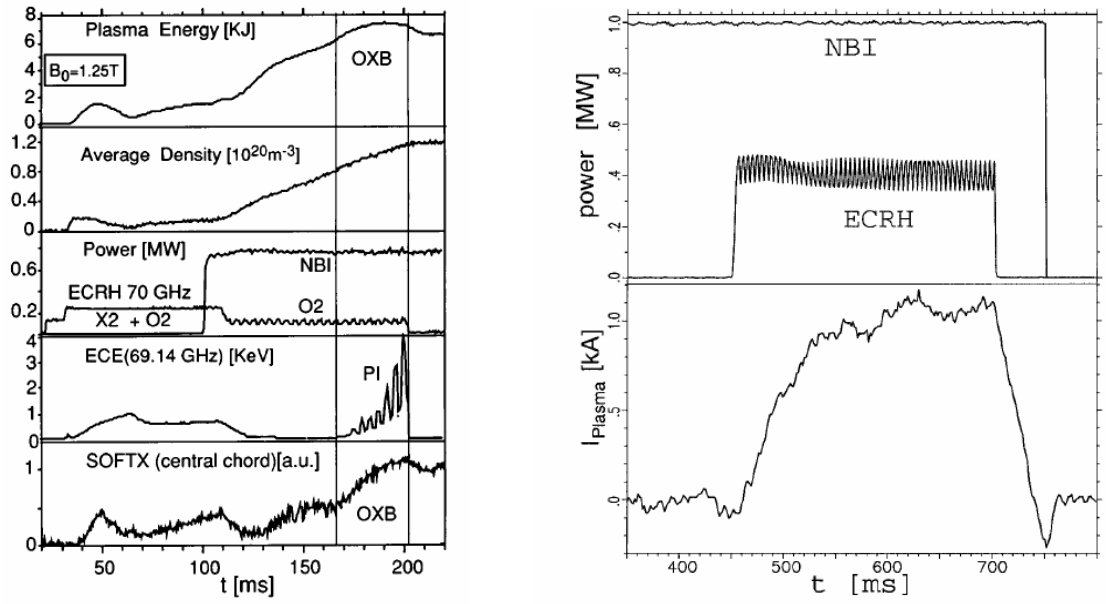

Fig. 2: Experiments on EBW heating (left) and EBW current drive (right) on the W7-AS stellarator. The left panel shows the signature of OXB EBW heating: as the density passes the O-mode cutoff density the stored energy increases to rise while the parametric decay instablity appears on the ECE channel, modulated with the EC power. The right panel shows the increase in plasma current due to EBW curremt drive in an overdense plasma.

The first successful experiments according to this scheme were carried out in the W7-AS stellarator [13] where all elements of the scheme described above could be verified experimentally. The O-X conversion was verified via studying the angular dependence of the heating efficiency and the X-B conversion due to the characteristic parametric decay instability into multiples of the lower hybrid frequency. An example is shown in the right panel of Fig. 2. Clear heating effects were seen both with and without resonance inside the UHR layer (the latter being attributed to resistive dissipation of the wave trapped inside the

UHR that forms an annulus in this case). From power balance, a transmission efficiency as high as 70% was inferred and finally, also the reduction of transmission due to an increase in fluctuation amplitude could be demonstrated. Good agreement was found between modeling the optimum injection angle and the experimental results. Finally, as shown in the right panel of Fig. 2, also current drive by using Bernstein waves created by the OXB scheme was demonstrated in W7-AS [16]. The results were consistent with the higher CD efficiency compared to usual ECCD schemes, as quoted for COMPASS-D above.

Another stellarator using EBW is CHS and the results confirm the W7-AS findings. In a recent paper [17], an increase in stored energy of as high as 30% by injecting 400 kW of EBW power at 54.5 GHz into a discharge heated with 800 kW NBI was demonstrated while the density was increased up to 8 x 10^{19} m^{-3} (the O-mode cutoff is at 3.8 x 10^{19} m^{-3} for 54.5 GHz), as can be seen in the left panel in Fig. 3. At this density, the discharge could only be sustained when EBW was injected, NBI alone would lead to a radiative termination. Variation of the injection angle showed a clear minimum in EC stray radiation, shown in the right panel of Fig. 3, coincident with a maximum in stored energy when the injection angle was close to the optimum calculated value. The increase in stored energy increased with EC power and showed a maximum when the magnetic field was tuned such that the EC resonance was on-axis, giving confidence in the OXB scheme being responsible for the increased stored energy. Finally, in CHS, an experimental variation of the polarization of the injected EC wave was also performed and showed highest efficiency when left-handed polarization was chosen, which is expected to convert best to the slow X-mode.

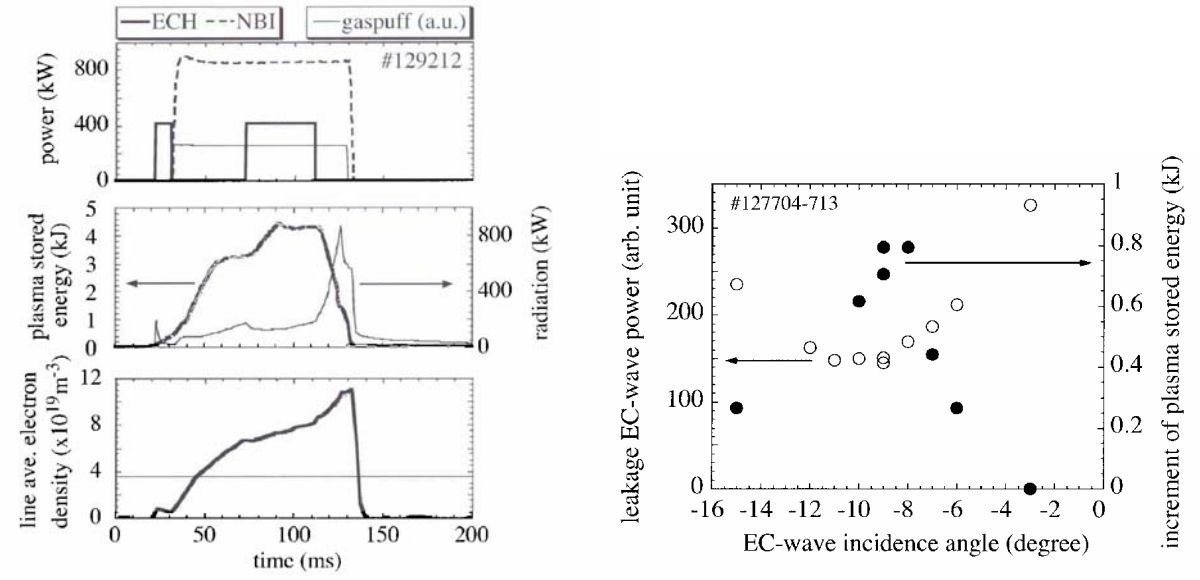

Fig. 3: OXB experiment in CHS: 400 kW of EC power sustains an overdense plasma up to twice the cutoff density (left). The right panel shows a maximum in stored energy increase, coincident with a minimum in EC stray power, during a scan of the injection angle.

The first demonstration of the OXB scheme in a conventional tokamak was achieved on TCV [18], where an Ohmic H-mode target plasma was successfully heated using OXB at the second harmonic. The absorbed power was estimated to be of the order of 60% at most, indicative of the O-X transmission efficiency. The optimum injection angle was calculated and measured, both in terms of maximum absorption and minimum stray radiation, with good agreement between the two. Since the plasma was in the H-mode regime, the effect of edge localized mode (ELM) perturbations on the OXB scheme could be studied. It was found that

the stray radiation level increased just after an ELM and the authors attributed that to the change in density profile due to the ELM. This highlights one of the drawbacks of OXB heating and current drive, namely its sensitivity to the magnetic configuration and the density profile, including the fluctuations. These do not exist for conventional ECRH and ECCD, and in that respect, OXB is more similar to LH or ICRH schemes, where similar sensitivity to the plasma (edge) conditions exist.

As pointed out above, Bernstein waves represent the only access to the electron cyclotron resonance in low field devices such as RFPs and STs. Thus, a continuously growing experimental effort has been made in spherical tori in the recent years, most notably in MAST [19] and NSTX [20]. However, the results so far are not as clear as in the stellarator devices. Measurements of electron Bernstein wave emission in NSTX show good agreement with the theoretical expectation in L-Mode plasmas at the fundamental frequency, but the second harmonic emission is substantially lower than predicted. In addition, during H-mode, there is a continuous decrease of the 1st harmonic emission with respect to the predicted value. A possible interpretation put forward is that the magnetic field configuration in the plasma edge changes considerably in H-mode due to the build-up of bootstrap current associated with the steep pressure gradient. More general, the large variability of the density gradient in H-mode (spherical) tokamaks may be a problem for the OXB scheme in these devices. However, recent experiments in MAST using a non-optimum frequency of 60 GHz have shown clear signatures of OXB heating verifying that in principle, it is possible to apply this scheme in STs. Also, Electron Bernstein Emission experiments were reported to better agree with theoretical predictions in MAST. Clearly, more work is needed here, also on the theoretical side, where a new challenge when applying the OXB scheme to spherical tori is that at the lower frequency, the wavelength is not necessarily small compared to the density gradient length as well as the spatial separation of UH and O-mode cutoff layer, so that ray tracing methods may not be appropriate any more. Finally, we note that for current ramp-up in STs, a large variation of edge conditions both in magnetic configuration and kinetic profiles is expected so that an in-situ adaptation of the launching angle, possibly by a feedback control similar to that shown in the X3 experiments in TCV (see Section 2.1), may be needed to exploit the scheme.

2.3 Synergy of ECRH and ECCD with LH waves

As pointed out above, the current drive efficiency of ECCD is usually much lower than that of LHCD due to the different phase space interaction mechanism. On the other hand, deposition of ECCD is very localized and usually quite well controlled from the exterior, e.g. by changing the launching angle. Experiments have therefore been conducted studying the synergy between LH and EC waves to combine the merits of both methods. Here, the idea is to generate a suprathermal electron fraction by LH waves on which the EC waves are absorbed, thus moving the interaction region of the EC waves in phase space to higher energies, thereby enhancing the CD efficiency.

A very convincing proof of this interaction was done on the FTU tokamak (see [21] and references therein), where it could be shown that O1 EC waves were absorbed in an LHCD preheated plasma that did not even contain the EC cold resonance. Two effects can lead to this downshifted absorption, namely the lowering of the cyclotron frequency by the relativistic mass increase and the Doppler shift due to finite $N_{||,ECCD}$. Assuming that the resonant electrons are created by LHCD and that their velocity is dominated by its parallel component, i.e. $v \approx v_{||} = c/N_{||,LHCD}$, we can re-write the resonance condition Eqn. (5) as

$$\frac{\nu_{ce0}}{\nu_{wave}} = \frac{N_{||,LHCD} - N_{||,ECCD}}{\sqrt{N_{||,LHCD}^{\ 2} - 1}} \qquad (9)$$

where ν_{ce0} is the cold resonance, i.e. calculated using $m_e=m_0$. In FTU, perpendicularly launched O-mode EC waves (i.e. $N_{||,ECCD} = 0$) at 140 GHz, for which the fundamental cold resonance is at 5 T, were absorbed up to 50% single pass in a plasma discharge with B_0= 7.2 T. For the FTU aspect ratio of 3, the cold resonance was indeed outside the plasma, but the downshift factor (9) using $N_{||,LHCD}$ = 1.52 in this particular experiment is 1.33 and thus we expect absorption at 6.7 T, which is located around normalized minor radius 0.1. In addition, an increase and widening of the hard X-ray emission profile was observed, demonstrating that the interaction indeed takes place at the high velocities generated by LHCD. Finally, it was also observed that the ECCD efficiency in these plasmas greatly exceeds the usual values, coming close to the efficiency typical for LHCD. This effect is usually referred to as 'synergy', i.e. the total current driven in a discharge with combined application of LHCD and ECCD is larger than the sum of the currents driven by the individual systems alone.

Concerning the quantitative characterization of this synergy, very clean experiments have been performed in the Tore Supra tokamak [22]. In these experiments, long pulse discharges (duration many times the current diffusion time scale) were carried out in which the OH transformer current was not changed, i.e. under conditions with $V_{loop} = 0$. Constant plasma current was initially sustained by feedback control of LHCD power ($N_{||,LHCD} \approx 2$). Then, EC power was injected in O-mode polarization for co-current drive ($N_{||,ECCD} \approx 0.5$ at the absorption region) at 118 GHz, corresponding to the cold resonance of 4.2 T (according to Eqn. (9) the absorption is then upshifted by about 20%). The feedback control on the plasma current reacts to this by reducing the LHCD power in order to keep the total current constant. An example is shown in the left panel of Fig. 4. One can immediately see that the reduction of LHCD power is comparable to the ECCD power, indicating similar CD efficiencies.

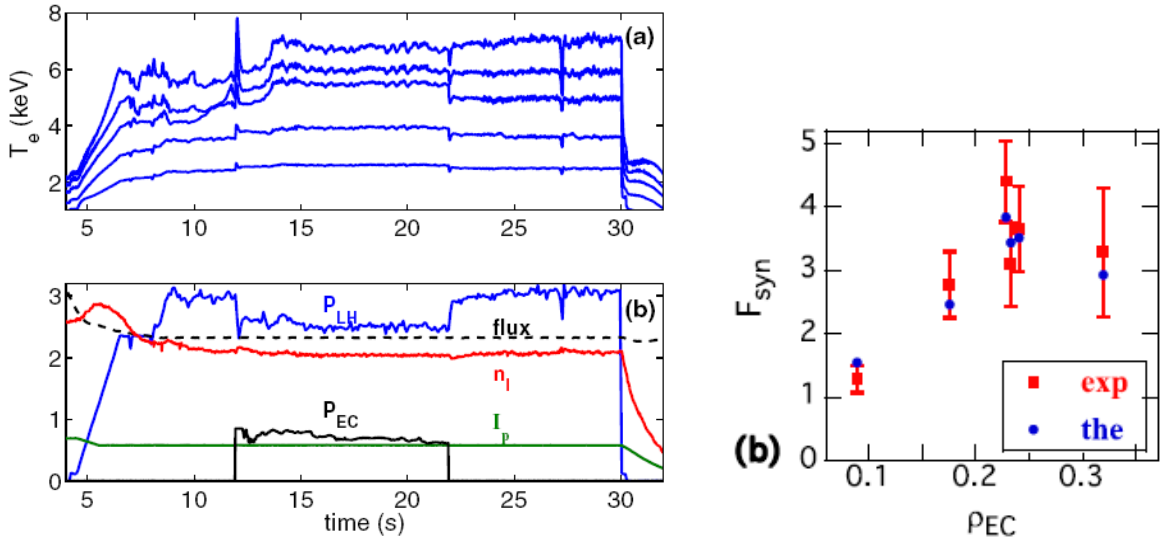

Fig. 4: Combined LHCD and ECCD in Tore Supra. The left panel shows the time evolution: I_p is kept constant by feedback controlling P_{LH} (no inductive CD). At the application of ECCD, P_{LH} is reduced considerably. In the right panel, the experimentally derived synergy factor $(I_{LHCD+ECCD}-I_{LHCD})/I_{EC}$ is shown together with predictions from kinetic modelling.

This qualitative finding has been analyzed in depth on Tore Supra together with kinetic modeling using a suite of experimentally benchmarked codes. By comparing the driven current by EC in the presence of LHCD to that predicted to be driven in the absence of LHCD, typical synergy factors of the ECCD efficiency of the order of 2-5 are found, as plotted in the right panel of Fig. 4. Here, the synergy factor is defined by $(I_{LHCD+ECCD}-I_{LHCD})/I_{ECCD}$, where $I_{ECCD+LHCD}$ is the current driven in the discharge with combined application while I_{LHCD} and I_{ECCD} refer to the current driven by LH or EC waves when the respective scheme is applied alone. The right panel in Fig. 4 also shows the predicted synergy effect obtained by applying kinetic modeling. Good agreement between experiment and prediction is found. The substantial increase in ECCD efficiency is explained by the combined effect of ECCD and LHCD in that ECCD acts to pull out low energy electrons form the Maxwellian distribution and LHCD then drives these electrons to high parallel velocities. Thus, the effect relies on an overlap of the interaction region of LHCD and ECCD in phase space. In addition, the overlap is also mandatory in real space, as can be seen by the variation of the synergy factor with ECCD deposition location in the right panel of Fig. 4.

While these experiments show that the interaction of LHCD and ECCD can be very beneficial and promises to combine the merits of both methods in common application, recent experimental findings on the TRIAM-1M tokamak [23] point out that more work in this area is needed to understand the variety of phenomena observed. Here, X1 low field side launch in the ctr-current direction ($N_{||,ECCD} = -0.3$) was used. As explained in the previous section, X1 waves lanched from the low field side cannot reach the resonance for thermal electrons, but the strong downshift when interacting with suprathermal electrons generated by LHCD can open a window between X-mode cutoff and the maximum absorption radius defined by $(\nu_{ce0}/\nu_{wave})_{max} = (1-N_{||,ECCD}^2)^{1/2}$. This condition can be derived from Eqn. (5) in a similar fashion as Eqn. (9), but this time assuming that $v_{||}/c = N_{||,ECCD}$, i.e. the suprathermal electrons travel with the same parallel velocity as the EC wave. Surprisingly, combining backward ECCD with forward LHCD can lead to an increase of the driven current. While this may be explained by a dominant Ohkawa current when the deposition is on the low field side, results with deposition on the mid-plane high field side, where virtually no trapped particles exist, call for a more refined theoretical explanation yet to be given.

3. Application of ECRH and ECCD for optimization of plasma stability

A very active area of application of ECCD is the optimization of plasma stability, making use of the ability of EC waves to drive localized currents. In toroidal fusion plasmas, MHD instabilities usually occur localized around so-called resonant magnetic surfaces, i.e. surfaces on which the field lines close up on themselves after q turns around the torus in toroidal direction, where q is the so-called safety factor. The resonant condition for an MHD mode is when $q=m/n$ where m and n, the poloidal and toroidal mode numbers are integer numbers characterizing the toroidal and poloidal periodicity of the mode. A particular class of MHD instabilities in tokamaks is the Neoclassical Tearing Mode NTM which is driven unstable by the loss of pressure driven current, the so-called bootstrap curent, inside the magnetic island associated with the mode. This mode limits the achievable pressure in standard tokamak discharges and may therefore be a major limitation to the achievable fusion power in future fusion reactors. Suppression of NTMs by ECCD is possible by replacing the missing bootstrap current by ECCD driven current.

By the time of the previous review [5], the suppression of ($m=3,n=2$) NTMs had been demonstrated in several tokamaks [24], [25], [26] and [27] and first experiments on partial (2,1) suppression had been carried out. Also, first attempts at feedback control of the

deposition had been made. Since then, full suppression of the (2,1) NTM has been demonstrated in several devices [27], [28], [29] and feedback control has been developed further. Based on this success, ECCD suppression of NTMs is now a major goal for the ITER ECCD system and recent experimental work has been geared towards establishing the physics base for the design of the ITER ECCD system with respect to this particular point. Below, we review the recent elements of this research where we restrict ourselves to the elements concerning mainly the application ECCD. The physics of NTMs themselves is not treated here in detail.

3.1 Progress in understanding the physics of NTM stabilization by ECCD

A first group of experiments is aimed at verifying the theoretically predicted approach to optimization of NTM stabilization. Theory predicts that only the helical current deposited inside the island has a stabilizing effect. In the limit of deposition width d bigger than island width W, this means that the current density rather than the total current should be maximized and has led to the definition of the figure of merit $\eta_{NTM} = j_{ECCD}/j_{bs}$ where j_{bs} is the bootstrap current density [30]. Based on [30], a criterion of $\eta_{NTM} > 1.2$ was defined as the ITER requirement [31], which is in rough agreement with an extrapolation of experimental results from ASDEX Upgrade, DIII-D and JT-60U [32]. Here, the biggest experimental uncertainty is at present the determination of the mismatch between ECCD deposition location and resonant surface [31], and this question will be addressed in the near future in detailed experiments in these devices. Since both I_{ECCD} and d usually increase with toroidal launch angle, but not with the same power, an optimum toroidal launch angle can be found that maximizes j_{ECCD}. Experiments in ASDEX Upgrade [28] have, by scanning the toroidal launch angle, convincingly verified this optimization strategy. It was found that the power requirement for complete (3,2) NTM suppression was indeed lowest when the current density was maximized, while at even higher launch angle and therefore higher I_{ECCD} but lower j_{ECCD}, the power requirement was found to increase. Similar results were also found when optimising the launch angle in JT-60U [29]. We note here that a narrower deposition profile is also predicted to be beneficial for sawtooth tailoring and first hints of this have recently been obtained on ASDEX Upgrade [33].

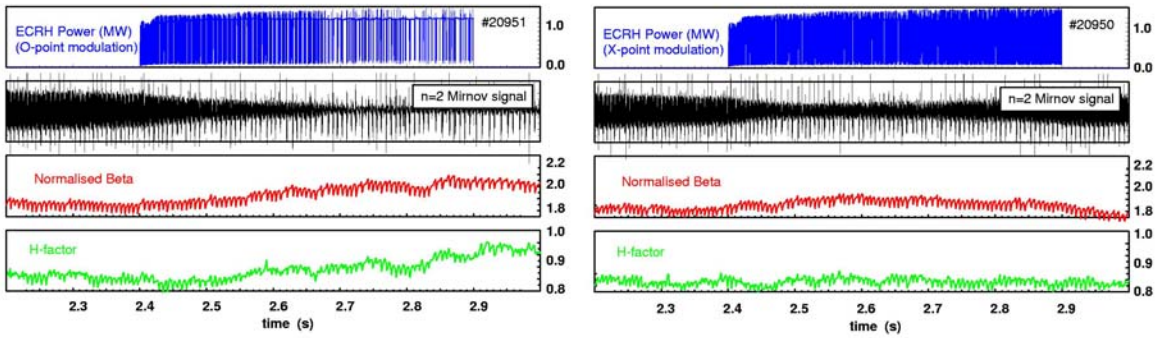

Fig. 5: NTM suppression with modulated ECCD injection in ASDEX Upgrade: modulation around the O-point of the magnetic island results in full suppression, accompanied by an increase in pressure (left panel), while modulation around the X-point fails to do so (right panel). In both discharges, the deposition is swept over the resonant surface by a B_t-ramp.

Another important point is that only helical current of the same helicity as the magnetic island has a stabilizing effect, so that current driven in the area of the island O-point is stabilizing while helical current around the X-point is predicted to have a destabilizing effect. Since NTMs often rotate with respect to the ECCD launcher, this calls in principle for a phased

injection of ECCD into the island O-point. Nevertheless, for $d < W$, which is mostly the case in present day experiments, the rapid parallel diffusion of the current carrying electrons along the flux surfaces of the magnetic island generates current of the correct helicity even for continuous injection, since the flux surface area around the O-point is smaller than around the X-point, so that a constant source will drive higher current density in the O-point. This is readily confirmed in the experiments, where DC injection into rotating islands is commonly used to fully suppress NTMs. However, for $d > W$, which is predicted to be the case during NTM suppression in ITER, the helical current will go to zero since without gradient in the current density across the island, the above mentioned averaging mechanism produces the same result around the O-point and around the X-point. It has thus been postulated that for $d > W$, modulation in phase with the O-point will substantially lower the power requirement for complete NTM suppression. This has recently been demonstrated experimentally in ASDEX Upgrade by using a toroidal launch angle larger than the optimum one to mimic the ITER situation with $d > W$. An example is shown in Fig. 5. Under these conditions, a clear difference in efficiency between X-point and O-point modulation was found, with O-point modulation being more efficient [34]. We note that phased injection around the X-point does have a stabilizing effect, which is thought to be due to the change in equilibrium current profile induced by the (0,0) component of the driven current. Similar results have been obtained on TEXTOR using islands induced by an external helical perturbation which can be rotated relative to the ECCD antenna [35]. Another effect not taken into account in most of the present modeling is the contribution of the heating due to ECRH in the island; this effect has clearly been demonstrated recently in TEXTOR experiments on classical tearing mode suppression [36].

3.2 Feedback controlled deposition for NTM suppression by ECCD

As outlined above, it is crucial for the success of NTM suppression by ECCD to deposit a localized current within the magnetic island, i.e. at the resonant surface of interest. For a routine application of ECCD suppression of NTMs, it is therefore necessary to develop schemes to feedback control the deposition location, since in practice, the resonant surface of interest can move due to changes in the tokamak current or pressure profile (the latter entering via the Shafranov shift). First attempts at this control were done in the DIII-D tokamak [27], where a so-called 'search and suppress' algorithm was applied to vary the deposition by a radial plasma shift or a change in B_t to detect the associated change in NTM amplitude and then adjust the deposition in steps to find the minimum mode amplitude. One drawback of this method is that the actuators used will not be available in superconducting fusion-grade plasmas und thus feedback control should be done via control of the launching mirror angle. This has been demonstrated successfully on JT-60U [37], where the correlation between ECE channels that detect the mode amplitude was used to track the position of the mode. This sensor, as well as the mode amplitude from Mirnov coils used in the previously described DIII-D experiment, has the disadvantage that feedback control is only possible when the NTM has already been triggered and can therefore not be used for preemptive ECCD, which has been shown in JT-60U to be very efficient in preventing the mode from onset [38]. Here, on-line equilibrium reconstruction of the position of the resonant surface is needed as a sensor. This has recently been implemented in DIII-D [39]. An example is shown in Fig. 6. The deposition is varied via B_t feedback such that also after (2,1) NTM suppression, the position of the q=2 surface as predicted from on-line equilibrium reconstruction is tracked. As can be seen, the mode remains suppressed during the subsequent β_N-ramp up to the ideal MHD stability limit, but re-strikes immediately after ECCD is turned off. Finally, we note that also an algorithm that recognizes the occurrence of the mode and acts on the ECCD will be needed; this has been demonstrated recently in the FTU tokamak where gyrotrons were run in

modulated mode with low duty cycle and switched to high duty cycle modulation when the mode was detected [40]. The modulated operation was used to measure the ECCD deposition location by ECE, while the resonant surface was detected using an ECE correlation method. This approach has the advantage of not requiring any mapping in real space because it relies on ECE frequency information only. Recently, yet another method of controlling the deposition has been proposed, using similar or identical sightlines for ECE and ECCD [41]. This will be implemented in TEXTOR and ASDEX Upgrade in the near future.

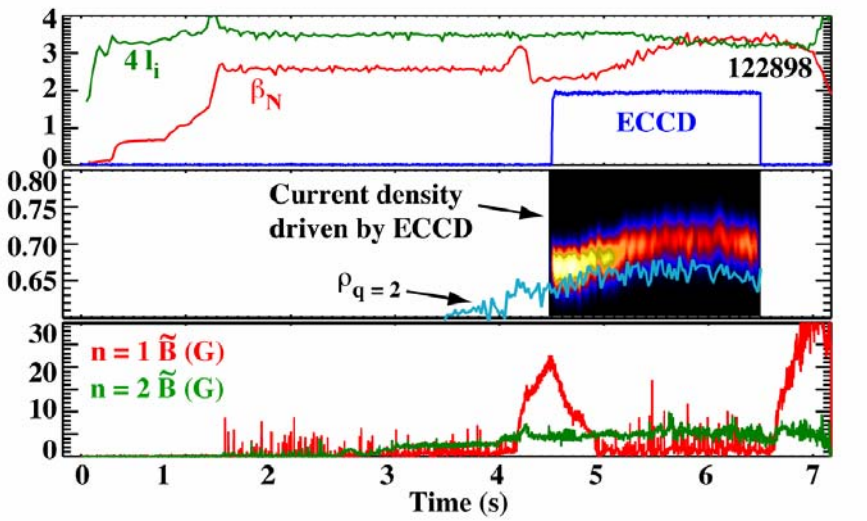

Fig. 6: (2,1) NTM suppression in DIII-D with feedback controlled deposition using on-line reconstruction of the q=2 resonant surface as sensor and B_t as actuator.

4. Summary and Outlook

In this review we have summarized recent progress in the area of experiments using ECRH and ECCD. The focus was on two very active areas of research using electron cyclotron waves, namely the development of new schemes for heating and current drive using EC waves, other than the well-established O1 and X2 schemes, and the application of ECCD for the stabilization of NTMs.

Concerning the development of new schemes, the main goals are to use EC waves at plasma densities above the cutoff density for the classical schemes and to enhance the CD efficiency. In the first area, the extension of O1 and X2 to O2 and X3 was discussed, which allows higher density to be accessed at the cost of incomplete first pass absorption. This has been addressed by maximizing the interaction of the beam on the first pass using top launch and feedback control of the injection angle. An in principle unlimited extension above the cutoff densities can be achieved using Electron Bernstein waves. The OXB scheme has been shown to be very well applicable in stellarators, where good agreement with theoretical predictions of beam propagation and absorption was found. In tokamaks and spherical tori, the situation is less clear. This is mainly attributed to the larger variability of edge conditions, both in terms of magnetic configuration and kinetic profiles. Clearly, the way to go is to apply some sort of feedback control of the launch angle in these devices, along the lines of the X3 scheme mentioned above. If successful, Bernstein waves could play a major role in the current ramp-up and sustainment in spherical tori, an area that is crucial for the further success of these devices.

In the area of increasing the CD efficiency, it has been shown that Bernstein waves can, as predicted by theory, have a higher CD efficiency than the classical schemes. Furthermore, it was shown that the synergy of LH waves and EC waves can lead to a localized current drive (as is the case for ECCD alone) with a CD efficiency close to that of LHCD (which is generally up to an order of magnitude higher than that of ECCD). Good agreement was found with modeling predictions of the interaction in electron phase space. After the convincing proof-of-principle, the next step should be to use this scheme for physics applications such as ITB control or MHD mode stabilization, again implemented in some sort of feedback loop. A convincing proof could even promote this scheme for application in next-step devices, for which it is at present not considered.

In the area of NTM suppression by ECCD, clear progress in understanding the various physics elements has been made. It is now clear that the optimization strategy of maximizing j_{ECCD}/j_{bs} for conditions under which $d > W$ holds is successful and that in these conditions, also phased injection of ECCD into the O-point of the island has an advantage over continuous injection into a rotating mode. Elements of a feedback scheme for NTM control have been demonstrated in various devices and it is now time to combine these and demonstrate reliable NTM control in an automated system. Since various approaches concerning sensors, actuators and control strategies exist, a careful analysis of the capabilities of the individual elements has to be done to estimate the system performance, but in the end, an experimental confirmation will be needed before applying it to a next-step device such as ITER.

5. References

[1] V. Erckmann and U. Gasparino, Plasma Phys. Control. Fusion **36** (1994) 1869-1962.

[2] R. Prater, Phys. Plasmas **11** (2004) 2349-2376.

[3] K. Sakamoto, this issue.

[4] R. Olstad and J. Doane, this issue.

[5] T. C. Luce, IEEE Transactions on Plasma Science **30** (2002) 734-752.

[6] N. Fisch and A. Boozer, Phys. Rev. Lett. **45** (1980) 720-722.

[7] S. Alberti et al., J. Phys.: Conf. Series **25** (2005) 210-222.

[8] L. Porte et al., Proc. of the 21st IAEA Fusion Energy Conference, Chengdu, China (2006) Paper EX/P6-20.

[9] G.M.D. Hogeweij et al., Nucl. Fusion **44** (2004) 533-541.

[10] H. Laqua et al., 22nd EPS Conference on Controlled Fusion and Plasma Physics, Bournemouth, (1995) I357-I360.

[11] O. Mangold et al., Proc. of 29th Joint Int. Conf. on Infrared and Millimeter Waves and 12th Int. Conf. Terahertz Electronics in Karlsruhe (2004), ISBN 0-7803-8490-3, 717 - 718

[12] V. Shevchenko et al., Phys. Rev. Lett. **89** (2002) 265005.

[13] H. Laqua et al., Phys. Rev. Lett. **78** (1997) 3467-3470.

[14] A. Litvak et al., Phys. Lett. A **188** (1994) 188.

[15] H.P. Laqua, to appear in Plasma Phys. Controlled Fusion (2007).

[16] H. Laqua et al., Phys. Rev. Lett. **90** (2003) 075003.

[17] Y. Yoshimura et al., this issue.

[18] A. Mück et al., this issue.

[19] V. Shevchenko et al., this issue.

[20] S.J. Diem et al., Rev. Sci. Instruments **77** (2006) 10E919

[21] C. Sozzi et al., J. Phys.: Conf. Series **25** (2005) 198-209.

[22] G. Giruzzi et al., Phys. Rev. Lett. **93** (2004) 255002.

[23] H. Zushi et al., this issue.

[24] H. Zohm et al., Nucl. Fusion **39** (1999) 577.

[25] G. Gantenbein et al., Phys. Rev. Lett. **85** (2000)1242.

[26] A. Isayama et al., Plasma Phys. Control. Fusion **42** (2000) L37.

[27] R.J. La Haye et al., Phys. Plasmas **9** (2002) 2051.

[28] M. Maraschek et al., Nucl Fusion **45** (2005) 1369.

[29] A. Isayama et al., Proc. of the 21st IAEA Fusion Energy Conference, Chengdu, China (2006) Paper EX/P4-1a.

[30] R. Perkins et al., Poster presented at the 42nd APS/DPP annual meeting, Quebec, Canada (2000).

[31] H. Zohm, Proc. 14th Joint Workshop on ECE and ECRH, Santorin, Greece (2006).

[32] R.J. La Haye, Nucl. Fusion **46** (2006) 451-461.

[33] H. Zohm et al., accepted for publication in Nucl. Fusion (2007).

[34] M. Maraschek et al., Phys. Rev. Lett. **98** (2007) 025005.

[35] E. Westerhof et al., Nucl. Fusion **47** (2007) 85-90.

[36] I. Classen et al., Phys. Rev. Lett **98** (2007) 035001.

[37] A. Isayama et al., Proc. 19th IAEA Fusion Energy Conf., Lyon, (2002) IAEA-CN-94/EX/C2-2.

[38] K. Nagasaki et al., Nucl. Fusion **43** (2003) L7-L10.

[39] R. Prater et al., Proc. of the 21st IAEA Fusion Energy Conference, Chengdu, China (2006) Paper EX/P4-2.

[40] J. Berrino et al., IEEE Transactions of Nuclear Science **53** (2006) 1009-1014.

[41] E. Farshi et al., 2nd IAEA TM on ECRH Phys. and Techn. for ITER, Seeon, Germany, http://www.ipp.mpg.de/tmseeon/ (2003).